ISSN 1063-7826, Semiconductors, 2015, Vol. 49, No. 3, pp. 352–357. © Pleiades Publishing, Ltd., 2015.
Original Russian Text © E.A. Evropeytsev, S.V. Sorokin, S.V. Gronin, I.V. Sedova, G.V. Klimko, S.V. Ivanov, A.A. Toropov, 2015, published in Fizika i Tekhnika Poluprovodnikov, 2015, Vol. 49, No. 3, pp. 364–369.

SEMICONDUCTOR STRUCTURES, LOW-DIMENSIONAL SYSTEMS, AND QUANTUM PHENOMENA

Optical Studies of Carriers' Vertical Transport in the Alternately-Strained $ZnS_{0.4}Se_{0.6}$/CdSe Superlattice

E. A. Evropeytsev^, S. V. Sorokin, S. V. Gronin, I. V. Sedova, G. V. Klimko, S. V. Ivanov, and A. A. Toropov

Ioffe Physical-Technical Institute, Russian Academy of Sciences, St. Petersburg, 194021 Russia

^e-mail: evropeitsev@beam.ioffe.ru

Submitted July 10, 2014; accepted for publication August 25, 2014

Abstract—We present the results of theoretical modelling and experimental optical studies of the alternatively-strained CdSe/ZnS_ySe_{1-y} ($y = 0.4$) superlattice (SL) with effective band-gap $E_g^{\text{eff}} \sim 2.580$ eV and a thickness of ~300 nm, which was grown by molecular-beam epitaxy on a GaAs substrate. The thicknesses and composition of the layers of the superlattice are determined on the basis of the SL minibands parameters calculated implying both full lattice matching of the SL as a whole to a GaAs substrate and high efficiency of photoexcited carriers transport along the growth axis. Photoluminescence studies of the transport properties of the structure (including a superlattice with one enlarged quantum well) show that the characteristic time of the diffusion of charge carriers at 300 K is shorter than the times defined by recombination processes. Such superlattices seem to be promising for the formation of a wide-gap photoactive region in a multijunction solar cell, which includes both III–V and II–VI compounds.

DOI: 10.1134/S1063782615030070

1. INTRODUCTION

At present, a promising trend in the development of photovoltaic devices is the engineering of multijunction solar cells, which contain tunnel-connected subelements based on pseudomorphic layers of III–V and II–VI semiconductor compounds [1]. It is expected that the integration of photoactive III–V *p–n* junctions and II–VI junctions with wider gaps will make it possible to increase the efficiency of energy conversion as a result of more optimal capturing of the solar spectrum in comparison with multijunction solar cells based only on III–V compounds. A potentially suitable material for the fabrication of a II–VI subelement is the $Zn_{1-x}Cd_xS_ySe_{1-y}$ solid solution, and actual problem is development of the fabrication technology of pseudomorphic $Zn_{1-x}Cd_xS_ySe_{1-y}$ layers (on the GaAs substrate) with a widely varying band gap E_g, low density of defects, and good transport of photoexcited charge carriers promising. Using the Vegard law and the published parameters of materials, it can be shown that the $Zn_{1-x}Cd_xS_ySe_{1-y}$ is lattice-matched to GaAs in the composition region (x, y) from (0, 0.06) to (0.59, 1). In this range, E_g first decreases from ~2.75 eV (at 300 K), attains the smallest value of ~2.67 eV at the composition (0.56, 0.32), after which it increases to ~2.78 eV. Since the flux of photons from the solar spectrum decreases with increasing energy in the range under consideration, solid solutions with the smallest E_g (and, consequently, with a fairly high content of sulfur and cadmium) are of most practical interest.

The reproducible growth of high-quality $Zn_{1-x}Cd_xS_ySe_{1-y}$ by the method of molecular-beam epitaxy (MBE) is a fairly complex technological problem. It was previously shown that the fabrication of short-period ZnCdSe/ZnSSe superlattices (SLs) instead of a quaternary solid solution makes it possible to better control the growth process and reproducibly obtain the given values of the effective band gap (E_g^{eff}) and of the lateral lattice parameter [2]. In this publication, we report the results of theoretical simulation and experimental optical studies of a pseudomorphous CdSe/ZnSSe SL on a GaAs substrate with an effective band gap of ~2.58 eV (at 300 K). In Section 2, we describe the method of calculation of the SL parameters optimal from the point of view of minimization of the band gap, lattice-matching to the GaAs substrate, and the provision of the effective vertical transport of electrons and holes. Section 3 is devoted to the description of experimental samples and methods of measurements. In Section 4, we report experimental data on the optical and transport properties of the SL, obtained as a result of measuring the temperature dependences of the photoluminescence (PL) related to the SL and to the extended quantum well built into the SL. Section 5 sums up the results of our studies.

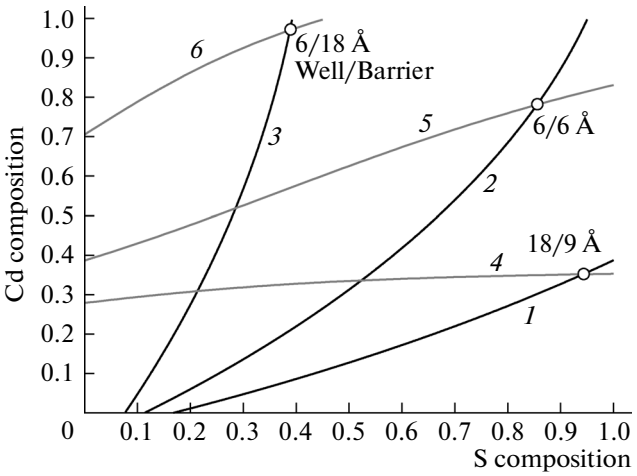

Fig. 1. Composition dependences of the contents of the ZnSSe/ZnCdSe SL layers corresponding to the condition $E_g^{\text{eff}} = 2.5$ eV (curves *1–3*) and to the condition of lattice matching to the GaAs substrate (curves *4–6*). Dependences *1–3* correspond to well/barrier thicknesses of 18 : 9, 6 : 6, 6 : 18 Å, respectively. Dependences *4–6* are drawn for ratios between the thicknesses of wells and barriers equal to 2 : 1, 1 : 1, and 1 : 3, respectively.

2. CALCULATION OF THE PARAMETERS OF OPTIMIZED SUPERLATTICES

2.1. ZnCdSe/ZnSSe Superlattices

Our calculation of the geometric parameters of the ZnCdSe/ZnSSe SLs includes determination of the thicknesses and compositions of the SL layers, at which the effective band gap E_g^{eff} of the SL takes values of 2.5–2.6 eV and at which the SL as a whole is lattice-matched to GaAs. The efficiency of the vertical transport of carriers is estimated on the basis of the calculated widths of lowest-energy electron and hole minibands in the SL. In this case, the critical parameter is the width of the thinnest miniband of heavy holes.

Relations between the thicknesses and compositions of the quantum-well (QW) layers at which the SL is lattice-matched to the GaAs substrate are found from the condition

$$a_{\parallel} = a_{\text{GaAs}}, \quad (1)$$

where $a_{\text{GaAs}} = 5.6533$ Å is the lattice parameter of GaAs and $a_{\parallel}$ is the lateral lattice parameter of layers of the hypothetical free-standing superlattice; this parameter is determined from the expression

$$a_{\parallel} = \frac{\sum a_i G_i h_i}{\sum G_i h_i}, \quad (2)$$

where a_i is the equilibrium lattice parameter, G_i is the shear modulus, h_i is the thickness of the ith layer, and summation is performed over all SL layers. Figure 1 (dependences *4–6*) shows the compositions of the SL layers corresponding to the fulfillment of condition (1) at various relations between the thicknesses of the wells and barriers. In choosing the layer thickness, it is also necessary to take into account that, for growth in the pseudomorphous mode, the thickness of each layer should be smaller than the critical thickness h_c, which depends on the lattice mismath between the layer and substrate. For the range of compositions under consideration, these thicknesses amount to several monomolecular layers (MLs).

The parameters of the SL minibands were calculated for a temperature of 300 K within two-band model in the method of smooth envelope functions. The parameters of the binary compounds used in the calculations are listed in the table. In calculations of the SL band diagram, we first determined the values of E_g for ZnS_ySe_{1-y} and $Zn_{1-x}Cd_xSe$. In this case, we used parabolic interpolation with the bowing parameter equal to 0.43 and 0.3, respectively. Then, within the Van de Walle theory [4], we calculated the variations in the band gap as a result of deformation of the SL layers with the SL grown pseudomorphously on the GaAs substrate. The obtained values of the band gaps $E_g^{e\text{-}hh}$ and $E_g^{e\text{-}lh}$ (separating the conduction band from the heavy- and light-hole subbands, respectively) were used in calculating the band offsets at the interfaces of $Zn_{1-x}Cd_xSe/ZnS_ySe_{1-y}$. The offset in the valence band of heavy holes $\Delta E_{v,\,hh}$ at the $Zn_{1-x}Cd_xSe/ZnS_ySe_{1-y}$ interfaces was determined using the transitivity rule:

$$\Delta E_{v,\,hh}(A/C) = \Delta E_{v,\,hh}(A/B) + \Delta E_{v,\,hh}(B/C); \quad (3)$$

here, A is ZnCdSe, B is ZnSe, and C is ZnSSe. The offsets of the valence band $\Delta E_{v,\,hh}$ at the interface between the ternary solutions and ZnSe (see expression (3)) were determined using the following phenomenological relations [5]:

$$\Delta E_{v,\,hh}(\text{ZnCdSe/ZnSe}) = 0.24(E_g^{\text{ZnCdSe}} - E_g^{\text{ZnSe}}), \quad (4)$$

$$\Delta E_{v,\,hh}(\text{ZnSSe/ZnSe}) = 1.00(E_g^{\text{ZnSSe}} - E_g^{\text{ZnSe}}). \quad (5)$$

The potential of the bottom of the conduction band E_c was found in each layer as the sum of the potential of the top of the valence band for heavy holes $E_{v,\,hh}$ and the band gap $E_g^{e\text{-}hh}$; the potential of the top of the valence band for light holes was found as the difference $E_c - E_g^{e\text{-}lh}$.

Figure 1 shows compositions at which E_g^{eff} is equal to 2.5 eV (dependences *1–3*) for SLs with three different relations between the widths of the wells and barriers. The points of intersection of dependences *1–3* with dependences *4–6* correspond to the simultaneous fulfillment of conditions imposed on $a_{\parallel}$ and E_g^{eff}.

Parameters of binary compounds

	ZnSe	ZnS	CdSe	CdS
a_0, Å	5.6681	5.4093	6.0770	5.8250
C_{11}, Mbar	0.826 [3]	1.067 [4]	0.667 [3]	0.77 [5]
C_{12}, Mbar	0.498 [3]	0.666 [4]	0.463 [3]	0.539 [5]
a_c, eV	−4.170 [4]	−4.090 [4]	−2.625 [6]	−2.77 [7] + 0.92 [8]
a_v, eV	1.65 [4]	2.31 [4]	1.039 [6]	0.92 [8]
b, eV	−1.2 [4]	−0.8 [4]	−0.8 [6]	−1.07 [7]
Δ_{SO}, eV	0.43 [4]	0.07 [4]	0.43 [9]	0.079 [10]
m_e/m_0	0.16 [3]	0.34 [11]	0.13 [3]	0.14 [5]
m_{hh}/m_0	0.60 [3]	1.76 [12]	0.45 [3]	0.39 [5]
m_{lh}/m_0	0.145 [13]	0.23 [12]	0.145 [13]	0.18 [5]
E_g (300 K)	2.721	3.726	1.675	2.46

a_0 is the parameter of the lattice in the free state; C_{11} and C_{12} are the elastic constants; a_c, a_v, and b are the deformation potentials; Δ_{SO} is the energy of the spin–orbit splitting; m_e, m_{hh}, and m_{lh} are the effective masses of electrons, heavy holes, and light holes, respectively; and m_0 is the mass of a free electron.

For example, for a ZnSSe(6 Å)/ZnSe(6 Å) SL, both these conditions are fulfilled at a S content of 0.85 and a Cd content of 0.78 simultaneously. At these parameters, the calculated width of the miniband of heavy holes is quite large (~50 meV). As the thickness of the wells (barriers) is increased, the given value of E_g^{eff} is attained at lower levels of the Cd (S) content; however, in this case, the width of the minibands determining the mobility of charge carriers along the growth axis decreases. As can be seen from Fig. 1 (dependences *3* and *6*), by increasing the barrier thickness compared with that of the wells, one can use the layers of the binary CdSe compound as QWs satisfying simultaneously the conditions for structural compatibility with GaAs and the value $E_g^{\text{eff}} = 2.5$ eV. Similarly, an increase in the QW thickness in comparison with the barrier thickness makes it possible to use the ZnS compound as the barrier material (see Fig. 1, dependences *1* and *4*). The use of layers of binary compounds in SLs is justified from the technological point of view since, in this case, the number of parameters, which should be controlled during the growth, is reduced. An additional advantage of CdSe wells is the possibility of calibrating the thickness of the CdSe layers in the grown structures via the position of the PL line from the extended ZnSe QW with incorporated CdSe plane of quantum dots (QDs) grown as a part of the same structure under the same conditions as the SL itself. Therefore, we chose the binary compound CdSe and ternary solid solution ZnSSe with a sulfur content of ~30–40% as the SL materials.

2.2. CdSe/ZnSSe Superlattices

For the chosen CdSe/ZnSSe system, we used the condition (1) to determine the ratio of well/barrier thicknesses depending on the sulfur content (Fig. 2a). Then, for the SL with determined parameters, we calculated the width of the heavy-hole miniband and E_g^{eff}. Figure 2b shows the parametric dependence of these quantities on the geometric parameters of the SL. In calculations of the miniband width we fixed the thickness of the QWs (barriers), while the remaining SL parameters, i.e., the barrier (QW) thicknesses and the content of sulfur were varied according to the dependence shown in Fig. 2a. The points of intersection of the dependences in Fig. 2b correspond to certain thicknesses of the wells and barriers and also to a certain composition of ZnSSe. The thicknesses of the CdSe wells used in the calculations do not exceed 2 ML since the critical thickness of plastic relaxation of the CdSe layer on the GaAs substrate with the formation of structural defects in self-formed CdSe islands (QDs) is ~3 ML, while the process of self-organization of the CdSe layer caused by elastic stresses begins already at thicknesses of 1.5–2 ML [14].

The following parameters of the CdSe/ZnSSe SL were chosen for experimental implementation: the thicknesses of the well and barriers were taken to be equal to 1.3 and 4 ML, respectively; the content of S in the barrier layer was taken as 0.41. For these parameters, the band gap $E_g^{\text{eff}} = 2.58$ eV (2.61 eV for light holes) and the width of the miniband for heavy holes is 67 meV. This miniband is partially overlapped with the wider miniband of light holes.

2.3. Superlattices with Smooth Heterointerfaces

It was shown previously that, during the growth of short-period CdSe/ZnSe SLs, thicker layers of the ternary ZnCdSe solid solution with a thickness of ~5 ML

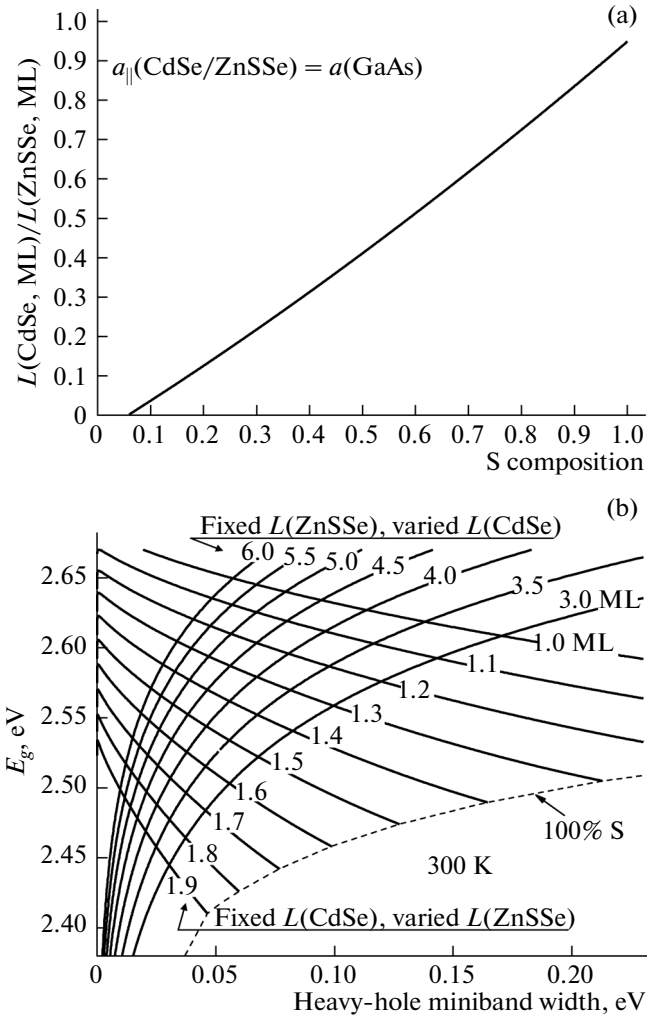

Fig. 2. (a) Dependence of the ratios between the thicknesses of the CdSe and ZnS_ySe_{1-y} on the content of sulfur; this dependence satisfies the condition for matching of the lattice parameter of the CdSe/ZnSSe system to that of GaAs. The thicknesses are expressed in the number of monolayers (MLs). (b) The dependence of the effective band gap on the width of the miniband of heavy holes in the CdSe/ZnS_ySe_{1-y} superlattice (SL) for the parameters, which change according to the dependence shown in Fig. 2a. The numbers *3–6* denote the fixed number of unstrained ZnS_ySe_{1-y} MLs; the numbers 1–1.9 denote the fixed number of fractional unstrained CdSe MLs. The dashed line represent the values attained at 100% content of S.

are formed instead of CdSe layers as a result of Cd and Zn diffusion [15]. In order to estimate the variation in E_g^{eff} as a result of spreading of the heterointerfaces between the SL layers, the above value was calculated taking into account the redistribution of the cadmium and sulfur concentrations along the growth axis of the structure. The distributions of Cd and S in separate layers were simulated in the form of Gaussian functions and were summed over 100 SL periods in such a way that the total (over the thickness) two-dimensional concentration of each element was not different from the nominal value for a SL with abrupt interfaces. The levels of dimensional quantization in a SL with smooth interfaces were determined using the transfer matrix method [16]. The values of the $Zn_{1-x}Cd_xS_ySe_{1-y}$ band gap (with layer deformation disregarded) was calculated using the formula

$$\begin{aligned} E_g(Zn_{1-x}Cd_xS_ySe_{1-y}) &= E_g(ZnSe)(1-x)(1-y) \\ &+ E_g(ZnS)(1-x)y + E_g(CdSe)x(1-y) \\ &+ E_g(CdS)xy - b^p(Zn_{1-x}Cd_xSe)(1-x)x(1-y) \\ &- b^p(ZnS_ySe_{1-y})y(1-y)(1-x) \\ &- b^p(Zn_{1-x}Cd_xS)(1-x)xy - b^p(CdS_ySe_{1-y})y(1-y)x, \end{aligned} \quad (6)$$

where the bowing parameters b^p for ZnCdSe, ZnSSe, ZnCdS, and CdSSe were taken equal to 0.3, 0.43, 0.827, and 0.54, respectively. Then, in the context of the Van-der-Walle theory, we calculated the band gaps taking into account layer deformation. The potential of the conduction-band bottom in the $Zn_{1-x}Cd_xS_ySe_{1-y}$ was determined relative to the bottom of the ZnSe conduction-band bottom using linear interpolation over the sulfur content between potentials of the $Zn_{1-x}Cd_xSe$ and $Zn_{1-x}Cd_xS$ conduction bands:

$$\begin{aligned} \Delta E_c(ZnCdSSe/ZnSe) &= (1-y)\Delta E_c(ZnCdSe/ZnSe) \\ &+ y\Delta E_c(ZnCdS/ZnSe). \end{aligned} \quad (7)$$

The offsets of the conduction band at the $Zn_{1-x}Cd_xSe$/ZnSe interfaces were determined as 76% (expression (4)) of the total band offset $E_g(Zn_{1-x}Cd_xSe)-E_g(ZnSe)$. The offsets of the conduction bands at the $Zn_{1-x}Cd_xS$/ZnSe interfaces were determined as 84% of the total band-offset at the $Zn_{1-x}Cd_xS$/ZnS interface [5] ($E_g(Zn_{1-x}Cd_xS)-E_g(ZnS)$) assuming that the conduction-band offset at the ZnS/ZnSe interface is negligibly small (expression (5)). The potential of the valence-band top in each layer was determined as the difference between the potential of the conduction-band bottom and the band gap determined within the Van-der-Walle model.

The width at half-height of the Gaussian distribution for the S concentration was chosen equal to the nominal thickness of the barrier layer (11.1 Å), which corresponds to a variation in the S content from 0.39 to 0.22. The width at half-height of the Gaussian distribution for the Cd concentration varied from 8 to 15 Å. Calculations for the CdSe(1.3 ML)/ZnS_ySe_{1-y}(4 ML) SL ($y = 0.41$) showed that broadening of the Cd and S profiles leads to a comparatively small decrease in E_g^{eff} to ~2.560 eV for heavy holes and to ~2.595 eV for light holes, and also to an increase in the lateral lattice parameter $a_{||}$ in the free state of the structure to

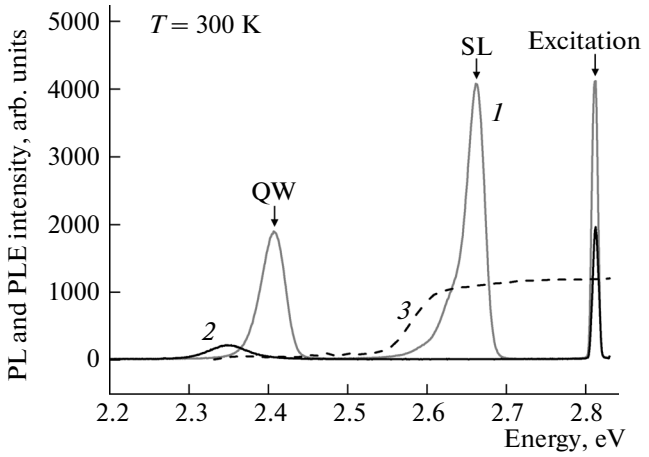

Fig. 3. Photoluminescence (PL) spectra measured at a temperature of 5.5 K (*1*) and at room temperature (*2*); the excitation PL spectrum (*3*) was measured at room temperature.

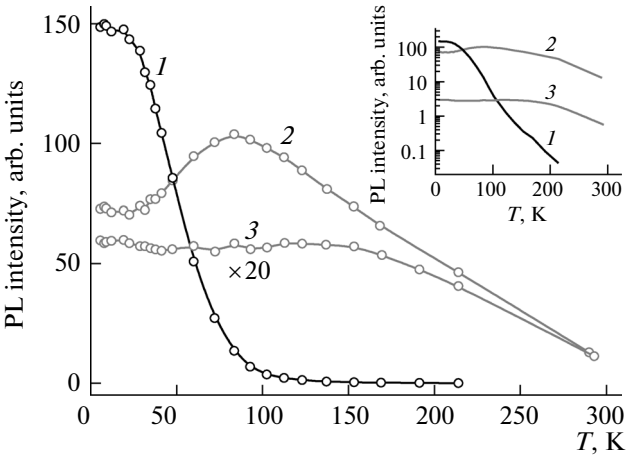

Fig. 4. Temperature dependence of the integrated intensity of PL from the SL (*1*), from a quantum well (QW) upon excitation with an energy higher than E_g^{eff} (*2*), and from a QW upon excitation with an energy lower than E_g^{eff} (*3*). The above dependences are shown on the semilogarithmic scale in the inset.

~5.695 Å, which corresponds to ~0.8% mismatch with the substrate.

3. EXPERIMENTAL

The structure was grown by the MBE method on a GaAs (001) substrate with GaAs and ZnSe epitaxial layers (~10 nm) at a temperature of 250°C; a double-chamber setup (Semiteq, Russia) was used. The 140 periods of ZnS_xSe_{1-x}/CdSe ($x \sim 40\%$) SLs (with a nominal thickness of the barriers and wells of 4 and 1.3 ML, respectively) were formed on the ZnSe buffer layer. Following the first 50 periods, a wider ZnSe(3 nm)/CdSe/ZnSe(3 nm) QW with a CdSe-layer thickness of 2.8–3.0 ML was formed. More detailed information on the conditions of growth and on the structural properties of the structure under consideration will be given in a separate publication.

In measurements of the temperature dependence of the PL and the PL excitation spectra, the sample was placed in a liquid-helium cryostat of the flow-through type. The temperature dependences were measured under conditions of above-barrier excitation with a photon energy of $E^{\text{exc}} = 2.817$ eV ($E^{\text{exc}} > E_g^{\text{eff}}$) or under selective excitation of the extended QW ($E^{\text{exc}} = 2.530$ eV, $E_g^{\text{QW}} < E^{\text{exc}} < E_g^{\text{eff}}$). As the excitation source, we used a halogen lamp and an MDR-12 monochromator, which cut out a narrow band from the lamp's spectrum with a resulting intensity on the order of 0.4 mW/cm^2. An Acton 2500 spectrometer and a cooled CCD camera were used for detection.

4. TEMPERATURE DEPENDENCES OF THE PHOTOLUMINESCENCE

The PL peaks related to the SL and QWs and located at 2.662 and 2.407 eV, respectively, are present in the PL spectrum of the structure under study; the spectrum was measured at a temperature of 5.5 K and at $E^{\text{exc}} > E_g^{\text{eff}}$ (see Fig. 3, curve *1*). As the temperature is elevated to 300 K, the PL related to the SL becomes much less intense (Fig. 3, curve 2), which can be attributed to the thermal activation of photoexcited charge carriers in the SL and their capture at the extended QW. In order to study changes in the vertical transport of carriers as the temperature is varied, we measurethe d the temperature dependence of PL of the structure.

Figure 4 shows the temperature dependence of the PL (related to the SL) integrated intensity (I^{SL}, curve *1*) and the PL related to the extended QW (I^{QW}, curve *2*). In the case of optical excitation with a photon energy of $E^{\text{exc}} > E_g^{\text{eff}}$, the majority of the electron–hole pairs are generated in the SL; then, a fraction of charge carriers diffuses to the extended QW. The value of the ratio $I^{\text{QW}}/I^{\text{SL}}$ (at $E^{\text{exc}} > E_g^{\text{eff}}$) is determined by the diffusion coefficient of charge carriers [17] and, consequently, characterizes the efficiency of the vertical transport.

A small value of the ratio $I^{\text{QW}}/I^{\text{SL}}$ and a slight dependence of the PL intensity (Fig. 4) and also the dependences of the position and width of the PL peaks (Fig. 5) on temperature in the range of 5–30 K are attributed to the localization of photoexcited charge carriers (or excitons) at fluctuations of the localizing

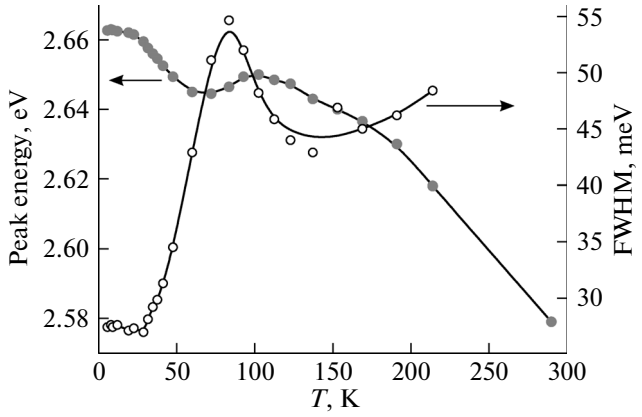

Fig. 5. Temperature dependences of the position (*1*) and width at half-height (*2*) for the peak of the PL from the superlattice. Solid lines are drawn for better clarity.

potential, which arise due to fluctuations in the composition of the ZnSSe solid solution and in the thickness of the layers composing the SL [18]. As the temperature is increased above ~30 K, the value of I^{SL} starts to decrease according to an exponential law; at the same time, the value of I^{QW} increases and attains a maximum at $T \approx 80$ K. An increase in I^{QW} with increasing temperature was observed only at an excitation energy higher than E_g^{eff} and is attributed to delocalization and an increase in the mobility of charge carriers along the SL growth axis. The temperature dependence of the position and width of the PL SL-related peak is nonmonotonous (Fig. 4), which is also indicative of an increase in the mobility of charge carriers as a result of their activation in the temperature range from ~30 to 100–130 K, which corresponds to a change conduction type from the hopping to band conductivity. The effective band gap of the SL at room temperature was determined from the PL excitation spectrum (Fig. 3, curve *3*) detected from the extended QW and amounted to $E_g^{eff} \approx 2.58$ eV.

5. CONCLUSIONS

We used the method of molecular-beam epitaxy to grow a $CdSe/ZnS_ySe_{y-1}$ superlattice (SL) with an effective band gap of $E_g^{eff} \approx 2.580$ eV (at 300 K). The SL parameters were chosen on the basis of an analysis of calculation of the band structure under the condition of matching the SL as a whole to GaAs with respect to the lattice parameter. According to calculations, in order to obtain $E_g^{eff} < 2.6$ eV and ensure effective vertical transport in the SL at 300 K, we used the ZnSSe solid solution with a fairly high content of sulfur (~40%). The value of E_g^{eff} in the obtained SL was determined by the excitation photoluminescence spectrum at room temperature and was found to be in good agreement with the calculated value. Optical studies of vertical transport in the SL showed that, at temperatures higher than 100–130 K, the times of diffusion of photoexcited electrons and holes along the growth axis of the structure are found to be much shorter than the characteristic recombination times.

ACKNOWLEDGMENTS

This work was partially supported by the Russian Foundation for Basic Research, grant no. 13-02-12216 ofi-m.

REFERENCES

1. Y. H. Zhang, S. N. Wu, D. Ding, S. Q. Yu, and S. R. Johnson, in *Proceedings of the 33rd IEEE Photovoltaic Specialists Conference* (San Diego, CA, USA, 2008).
2. T. V. Shubina, S. V. Ivanov, A. A. Toropov, G. N. Aliev, M. G. Tkatchman, S. V. Sorokin, N. D. Il'inskaya, and P. S. Kop'ev, J. Cryst. Growth **184–185**, 596 (1998).
3. H. J. Lozykowsky and V. K. Shastri, J. Appl. Phys. **69**, 3235 (1991).
4. C. van de Walle, Phys. Rev. B **39**, 1871 (1989).
5. S. Adachi, *Properties of Semiconductor Alloys: Group-IV, III–V and II–VI Semiconductors* (Wiley, Chippenham, 2009).
6. Yi-Hong Wu, IEEE J. Quantum Electron. **30**, 1562 (1994).
7. T. Nakayama, Solid State Electron. **37**, 1077 (1994).
8. A. Qteish and R. J. Needs, Phys. Rev. B **45**, 1317 (1992).
9. D. Olguin and R. Baquero, Phys. Rev. B **51**, 16891 (1995).
10. M. Willatzen, M. Cardona, and N. E. Christensen, Phys. Rev. B **51**, 17992 (1995).
11. H. Kukimoto and S. Shionoya, J. Phys. Chem. Sol. **29**, 935 (1968).
12. P. Lawaetz, Phys. Rev. B **4**, 3460 (1971).
13. V. Pellegrini, R. Atamasov, A. Tredicucci, F. Beltram, C. Amzulini, L. Sobra, L. Vanzetti, and A. Francioso, Phys. Rev. B **51**, 5171 (1995).
14. S. V. Ivanov, A. A. Toropov, T. V. Shubina, S. V. Sorokin, A. V. Lebedev, I. V. Sedova, P. S. Kop'ev, G. R. Pozina, J. P. Bergman, and B. Monemar, J. Appl. Phys. **83**, 3168 (1998).
15. R. N. Kyutt, A. A. Toropov, S. V. Sorokin, T. V. Shubina, S. V. Ivanov, M. Karlsteen, and M. Willander, Appl. Phys. Lett. **75**, 373 (1999).
16. A. K. Ghatak, K. Thyagarajan, and M. R. Shenoy, IEEE J. Quantum Electron. **24**, 1524 (1988).
17. F. Piazza, L. Pavesi, A. Vinattieri, J. Martinez-Pastor, and M. Colocci, Phys. Rev. B **47**, 10625 (1993).
18. A. A. Toropov, T. V. Shubina, S. V. Sorokin, A. V. Lebedev, R. N. Kyutt, S. V. Ivanov, M. Karlsteen, M. Willander, G. R. Pozina, J. P. Bergman, and B. Monemar, Phys. Rev. B **59**, 2510 (1999).

Translated by A. Spitsyn